

# Nanoscale

Accepted Manuscript



This is an *Accepted Manuscript*, which has been through the Royal Society of Chemistry peer review process and has been accepted for publication.

*Accepted Manuscripts* are published online shortly after acceptance, before technical editing, formatting and proof reading. Using this free service, authors can make their results available to the community, in citable form, before we publish the edited article. We will replace this *Accepted Manuscript* with the edited and formatted *Advance Article* as soon as it is available.

You can find more information about *Accepted Manuscripts* in the [Information for Authors](#).

Please note that technical editing may introduce minor changes to the text and/or graphics, which may alter content. The journal's standard [Terms & Conditions](#) and the [Ethical guidelines](#) still apply. In no event shall the Royal Society of Chemistry be held responsible for any errors or omissions in this *Accepted Manuscript* or any consequences arising from the use of any information it contains.

## COMMUNICATION

## Hollow spherical gold nanoparticle superstructures with tunable diameters and visible to near-infrared extinction

Cite this: DOI: 10.1039/x0xx00000x

Received 00th January 2012,  
Accepted 00th January 2012Chen Zhang,<sup>†a</sup> Yong Zhou,<sup>†b</sup> Andrea Merg,<sup>a</sup> Chengyi Song,<sup>a</sup> George C. Schatz,<sup>\*b</sup>  
and Nathaniel L. Rosi,<sup>\*a</sup>

DOI: 10.1039/x0xx00000x

www.rsc.org/

**Hollow spherical gold nanoparticle superstructures with tunable sizes (~40 nm, ~70 nm and ~150 nm) and visible to near-infrared surface plasmon resonances (545 nm, 670 nm, and 740 nm) are prepared using a single peptide conjugate, C<sub>6</sub>-AA-PEP<sub>Au</sub> as the structure-directing agent. Computational models are developed to understand their optical properties.**

Hollow spherical nanoparticle assemblies<sup>1</sup> are attracting widespread interest from multiple research communities because of their potential use as theranostic materials,<sup>1e-h, 1j-n</sup> heterogeneous catalysts,<sup>1d</sup> and metamaterials.<sup>2</sup> Hollow spherical gold nanoparticle assemblies, for example, have shown promise for drug delivery and as agents for photothermal therapy,<sup>1e-h, 1j</sup> for the latter, structures absorbing in the near-infrared (NIR) window (~650-900 nm) are particularly relevant, because biological tissue does not significantly absorb in this region of the spectrum.<sup>3</sup> In addition, large spherical assemblies of gold nanoparticles are known to display a significant magnetic dipole response in the visible, an important property for 'perfect imaging'.<sup>2</sup> Spherical assemblies of catalytic nanoparticles can show improved properties compared to individual nanoparticles. For example, we recently demonstrated that hollow spherical CoPt nanoparticle superstructures exhibit enhanced catalytic properties compared to discrete, non-assembled CoPt nanoparticles.<sup>1d</sup> Here, we present straightforward methods for preparing hollow spherical gold nanoparticle superstructures having three different diameters: ~40 nm, ~75 nm, and ~150 nm. We report the size-dependent optical extinction properties for this class of nanoparticle assemblies, which are tunable from the visible and into the NIR, and we develop computational models to understand these important collective optical properties. This work provides a practical route for preparing a family of spherical nanoparticle superstructures having tailorable diameters and optical properties.

Our motivation for fabricating spherical nanoparticle assemblies derives not only from their potential practical importance, but also from a fundamental interest in designing nanoparticle superstructures and controlling their compositions, morphologies, structural metrics, and physical properties. It is understood that the

properties of nanoparticle superstructures originate from the size, shape, and compositions of the component nanoparticles as well as the precise organization of the nanoparticles within the superstructures.<sup>4</sup> In order to design and prepare unique nanoparticle superstructures and control their physical properties, we have developed a peptide-based method for directing the synthesis and assembly of inorganic nanoparticles.<sup>5</sup> Briefly, this method utilizes peptide conjugate molecules that are designed to not only bind to the surface of specific inorganic nanoparticles, but also direct the assembly of these nanoparticles into particular target nanoparticle superstructures. The peptide portion of the peptide conjugate molecule binds to the nanoparticle surface,<sup>6</sup> while an organic molecule (e.g. an aliphatic chain) tethered to the peptide's N-terminus influences the assembly of the peptide conjugate. We have successfully used this methodology to prepare a diverse collection of nanoparticle superstructures with tunable compositions, morphologies, metrics, and properties.<sup>1b-d, 5, 7</sup>

In 2010, we reported that C<sub>6</sub>-AA-PEP<sub>Au</sub> conjugates (C<sub>6</sub> = C<sub>6</sub>H<sub>11</sub>O, A = alanine, PEP<sub>Au</sub> = AYSSGAPMPPF)<sup>6b</sup> direct the synthesis and assembly of hollow spherical gold nanoparticle superstructures.<sup>1b</sup> These structures consisted of ~8 nm gold nanoparticles arranged in a monolayer shell around a spherical vesicular self-assembled peptide conjugate core. Unique aspects of these structures included their small diameter (~50 nm) and hollow interior, which pointed toward their potential application as nanoscale carriers for drugs or other cargo. After this initial report, we also demonstrated that BP-A<sub>x</sub>-PEP<sub>Au</sub> (C<sub>12</sub>H<sub>9</sub>CO-A<sub>x</sub>-AYSSGAPMPPF; x = 2 or 3; BP = biphenyl) could also direct the formation of spherical gold nanoparticle superstructures and that the number of additional alanine residues at the N-terminus (2 or 3) controls the diameter of the spherical superstructures (large, >100 nm or small, ~30 nm).<sup>1c</sup> Based on this prior work, we can fabricate hollow spherical nanoparticle superstructures with three different diameters; however, each superstructure requires synthesis of a unique peptide conjugate molecule, which is practically limiting. Ideally, a single peptide conjugate should be capable of directing the formation of spherical superstructures with different diameters, provided that one can control the assembly conditions of the peptide conjugate and the diameter of its resulting spherical soft assembly (micelle or vesicle, for example) and the synthetic conditions for preparing the

nanoparticle superstructure. In this report, we demonstrate that C<sub>6</sub>-AA-PEP<sub>Au</sub> can be used to direct the synthesis and assembly of three different size classes of hollow spherical gold nanoparticle superstructures. We highlight the role of synthesis and assembly conditions in controlling the diameter of the spheres; we use UV-Vis spectroscopy to study their diameter-dependent optical properties; and we develop computational models to understand their visible and NIR extinction.

Our sphere syntheses are straightforward and require minimal synthetic effort. The three principal components of the syntheses are i) the peptide conjugate (in this case C<sub>6</sub>-AA-PEP<sub>Au</sub>), which serves as the particle binding agent and as the structure-directing agent; ii) 4-(2-hydroxyethyl)-piperazineethanesulfonic acid (HEPES) buffer (pH = 7.3 ± 0.1), which serves as the medium for self-assembly and as the primary reducing agent for Au<sup>3+</sup>;<sup>6b, 8</sup> and iii) a solution of chloroauric acid in 1.0 M triethylammonium acetate buffer (HAuCl<sub>4</sub>/TEAA), which is the source of gold ions.<sup>1b</sup> These components are combined together in one pot to yield a product nanoparticle superstructure. In order to prepare batches of spherical nanoparticle superstructures having different average diameters using C<sub>6</sub>-AA-PEP<sub>Au</sub>, we reasoned that we would have to systematically vary conditions such as the concentrations of C<sub>6</sub>-AA-PEP<sub>Au</sub>, HEPES buffer, and HAuCl<sub>4</sub>/TEAA. Careful adjustment of these conditions should allow for control over the diameter of the spherical C<sub>6</sub>-AA-PEP<sub>Au</sub> soft assembly that would ultimately serve as the underlying ‘template’ onto which the nanoparticles would assemble.

We began by studying the effect of HEPES buffer concentration on the soft assembly of a fixed amount of C<sub>6</sub>-AA-PEP<sub>Au</sub>. We dispersed 1.87 × 10<sup>-8</sup> mol C<sub>6</sub>-AA-PEP<sub>Au</sub> in 125 μL of four different concentrations of HEPES buffer (0.1, 0.05, 0.01, and 0.005 M) and studied their assemblies using transmission electron microscopy (TEM). At specific time points, samples of each solution were spotted onto formvar-coated copper TEM grids and stained using phosphotungstic acid. At the highest concentration of HEPES (0.1 M), no assemblies were observed, even after 1 week of incubation at room temperature. Large spherical structures (~500 nm diameter) were observed for the 0.05 M sample after 1 day, and a distribution of spherical structures of different diameters were observed after 6 hours and 30 minutes for the 0.01 M and 0.005 M samples, respectively (Fig. S1†). From these data, we can conclude that the assembly of C<sub>6</sub>-AA-PEP<sub>Au</sub> occurs more rapidly at lower HEPES concentrations than at higher concentrations. From previous studies,<sup>1b-4,5,7</sup> we determined that the HEPES buffer assists in dissolving the peptide conjugates; therefore, we reason that the conjugates assemble more rapidly at lower HEPES concentrations because they are less soluble at these concentrations. We concluded that HEPES concentration is an important variable that influences the assembly of C<sub>6</sub>-AA-PEP<sub>Au</sub>.

We next studied the assembly of C<sub>6</sub>-AA-PEP<sub>Au</sub> dissolved in a fixed amount and concentration of HEPES buffer (125 μL, 0.05 M) and with the addition of a fixed amount of HAuCl<sub>4</sub>/TEAA (0.6 μL of a 0.1 M solution of HAuCl<sub>4</sub> in 1.0 M TEAA buffer, pH = 7.0). After 30 minutes of incubation at room temperature, we observed large spherical assemblies (diameter = 109 ± 21 nm) at C<sub>6</sub>-AA-PEP<sub>Au</sub> concentrations between 100 and 150 μM and smaller spherical assemblies (diameter = 27 ± 8 nm) at C<sub>6</sub>-AA-PEP<sub>Au</sub> concentrations between 25 and 75 μM (Fig. S2†). After 4 hours of incubation, we only observed smaller spherical assemblies for each of the studied peptide conjugate concentrations. In the negatively-stained TEM images, we observe gold nanoparticles assembling around the

smaller assemblies. We concluded from these data that, at 0.05 M HEPES buffer concentration and in the presence of HAuCl<sub>4</sub>/TEAA, C<sub>6</sub>-AA-PEP<sub>Au</sub> will, over time, assemble into small spherical assemblies. Moreover, these assemblies will gradually be coated by gold nanoparticles. In fact, after 24 hours of incubation, all of the small spherical assemblies are fully coated with gold nanoparticles. These observations revealed a clear path to the synthesis and assembly of ‘small’ spherical nanoparticle superstructures. Thus, dissolving C<sub>6</sub>-AA-PEP<sub>Au</sub> (3.74 × 10<sup>-8</sup> mol) in 0.05 M HEPES buffer, adding an aliquot of HAuCl<sub>4</sub>/TEAA solution, and incubating the resulting mixture for 24 h at room temperature yielded small spherical nanoparticle superstructures with an average diameter of 40.4 ± 5.9 nm (Fig. 1a-b and Fig. S3†). The gold nanoparticles have an average diameter of 6.2 ± 0.9 nm and the average observable interparticle distance (gap) is 2.4 ± 0.6 nm (Fig. S3†). While we observe some free nanoparticles in the TEM images, the spherical superstructures comprise the major product. A negatively-stained image of a sample from the reaction after 4 hours of incubation indicates that the structures consist of nanoparticles surrounding peptide conjugate cores; we therefore describe the product as hollow spherical nanoparticle superstructures (Fig. S4†).

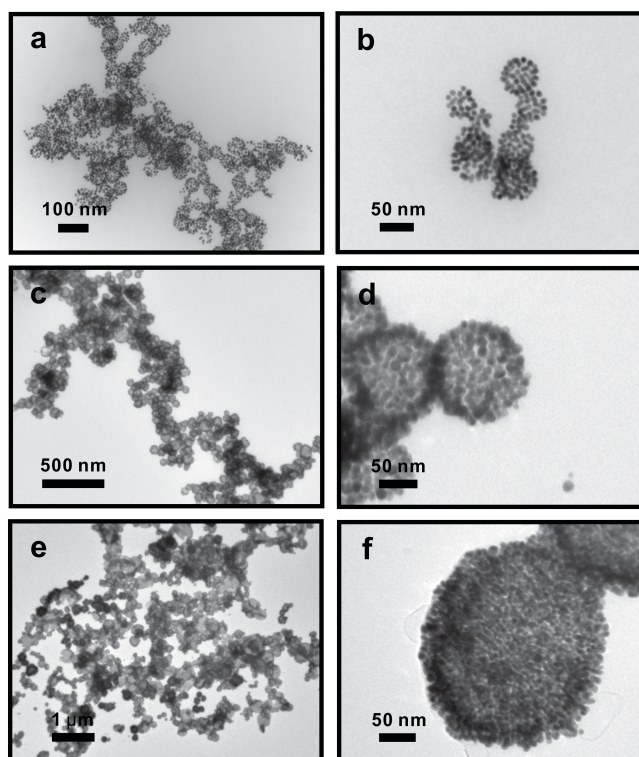
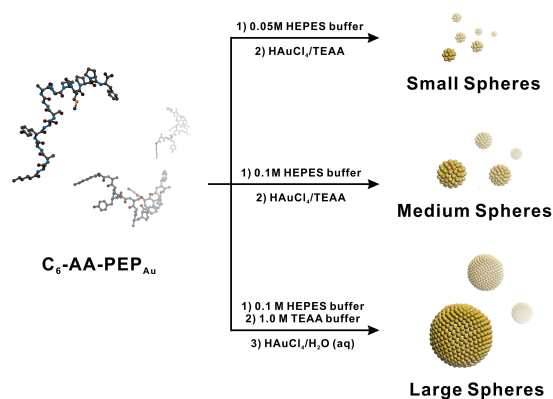


Fig. 1. TEM images of hollow spherical gold nanoparticle superstructures. (a,b) Small spheres, 40.4 ± 5.9 nm, (c,d) medium spheres, 75.3 ± 12.4 nm, and (e,f) large spheres, 149.7 ± 30.8 nm.

While we do not observe C<sub>6</sub>-AA-PEP<sub>Au</sub> assemblies in 0.1 M HEPES buffer (*vide supra*), we do observe the formation of hollow spherical nanoparticle assemblies after the addition of HAuCl<sub>4</sub>/TEAA and subsequent incubation at room temperature (Fig. S5†). Because we do not observe peptide conjugate assembly prior to the addition of HAuCl<sub>4</sub>/TEAA, we suspect that C<sub>6</sub>-AA-PEP<sub>Au</sub> assembly and nanoparticle formation occur simultaneously and that nanoparticle synthesis and assembly is a coupled process; however, at this stage,

this is a hypothesis. Hollow spherical nanoparticle superstructures with average diameter of  $75.3 \pm 12.4$  nm were formed after dissolving  $C_6$ -AA-PEP<sub>Au</sub> ( $1.87 \times 10^{-8}$  mol) in 0.1 M HEPES (125  $\mu$ L), adding an aliquot of HAuCl<sub>4</sub>/TEAA, and incubating for 3 days at room temperature. To minimize aggregation of the product structures, cetyl trimethylammonium bromide (CTAB) was added to the solution after 3 days.<sup>9</sup> During optimization of the synthesis, we observed that very small differences in the amount of added HAuCl<sub>4</sub>/TEAA significantly affects structural factors such as particle size and particle density within the product. We found that smaller amounts of HAuCl<sub>4</sub>/TEAA yield more well-defined and well-dispersed spherical superstructures, while larger amounts of HAuCl<sub>4</sub>/TEAA yield aggregated superstructures that are more densely loaded with nanoparticles (Fig. S6†). Ultimately, we determined that the addition of 0.7  $\mu$ L of the HAuCl<sub>4</sub>/TEAA solution yields the most uniform product (Fig. 1c-d and Fig. S7†). The average size of the nanoparticles comprising these structures is  $8.5 \pm 1.5$  nm and the observable interparticle distance (gap) is  $1.5 \pm 0.3$  nm (Fig. S7†).

Having prepared both small ( $\sim 40$  nm) and medium ( $\sim 75$  nm) diameter spherical superstructures, we next explored the synthesis of larger spheres ( $>100$  nm) using the same  $C_6$ -AA-PEP<sub>Au</sub> peptide conjugate. We observed that  $C_6$ -AA-PEP<sub>Au</sub> assembles into large spherical assemblies (diameter =  $240 \pm 81$  nm) when dissolved in mixtures of 0.1 M HEPES and 1.0 M TEAA buffer (Fig. S8†), which stands in contrast to what we observed in pure 0.1 M HEPES (*vide supra*). When an aliquot of aqueous HAuCl<sub>4</sub> is added to the solution of  $C_6$ -AA-PEP<sub>Au</sub> in HEPES/TEAA, we again observe the formation of large spherical peptide conjugate assemblies (diameter =  $236 \pm 75$  nm, Fig. S9†) after 4 hours of incubation at room temperature. After 24 hours of incubation, large hollow spherical gold nanoparticle superstructures having an average diameter of  $149.7 \pm 30.8$  nm were observed (Fig. 1e-f, and Fig. S10†). These structures consist of gold nanoparticles with an average diameter of  $9.9 \pm 1.6$  nm and an average observable interparticle distance (gap) of  $1.6 \pm 0.3$  nm (Fig. S10†). We conclude that the particles assemble around the peptide conjugate spherical assembly based on examination of negatively-stained images of a sample taken from the reaction after 10 hours of incubation (Fig. S11†). The thickness of the gold nanoparticle shell suggests that  $\sim 2$  layers of nanoparticles surround the peptide conjugate core. In summary, we have shown that a single peptide conjugate,  $C_6$ -AA-PEP<sub>Au</sub>, can be used to prepare small, medium, and large spheres simply by modifying the synthesis and assembly conditions (Scheme 1).



Scheme 1. Direct preparation of hollow spherical gold nanoparticle superstructures with different diameters using  $C_6$ -AA-PEP<sub>Au</sub> (yellow spheres = Au nanoparticles).

Assemblies of plasmonic nanoparticles often exhibit emergent collective optical behavior dependent on the composition and structure of the assembly.<sup>10</sup> Moreover, continuous gold nanoshells grown on spherical silica bead templates are known to have NIR extinction.<sup>11</sup> We were keen to measure the absorption properties of the prepared hollow spherical nanoparticle superstructures and to understand the origin of these properties. The UV-Vis spectra for each sample were found to have maxima at 545 nm, 670 nm, and 740 nm, respectively (Fig. 2a), indicating substantial shifts from the isolated gold nanoparticle plasmon wavelength of 520 nm, and increasing red-shift with increasing superstructure size. The extinction peak for the small spheres was much narrower than that observed for the medium and large spheres, which both exhibited very broad extinction ranging from 500-950 nm. We attribute this broad signal to polydispersity of the samples and coupling between the surface plasmons of the individual nanoparticles. We note that the extinction maximum for the large spheres (740 nm) lies in the NIR, which may prove useful for biological applications.<sup>12,13</sup>

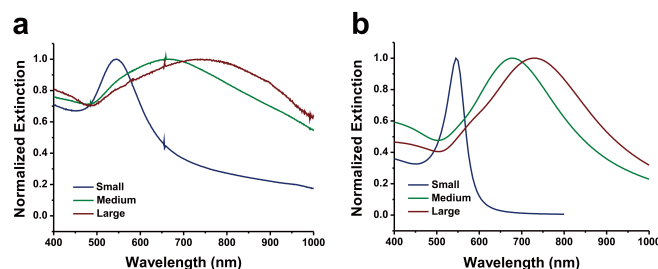


Fig. 2. (a) Experimental UV-Vis spectra of hollow spherical gold nanoparticle superstructures with varied sizes. The extinction maxima of small, medium and large gold nanospherical superstructures are observed at 545 nm (blue), 670 nm (green) and 740 nm (red) respectively. (b) Theoretical extinction spectra for the same superstructures, where the small superstructure is modeled using GMM (taking gap parameters from Table S1†) and the medium and large superstructures are modelled using Mie theory for a spherical metal shell structure.

Electrodynamics calculations have been carried out so as to relate the experimentally observed UV-Vis spectra to structural details of the assemblies. Given that the superstructures appeared to be composed of closely spaced but not necessarily overlapping gold particles, we first adopted the General Multiparticle Mie (GMM) method<sup>12</sup> for these calculations as this provides an exact solution to Maxwell's equations for an assembly of non-overlapping spherical nanoparticles.

The structural parameters used in the simulations are from the experimental measurements, as summarized in Table S1†. In the absence of structural details beyond what is pictured in the TEM images (e.g. Fig. 1), it is justified to assume that the nanoparticles are randomly distributed on the surface of the superstructure. This leads to approximately 32, 132, and 764 gold NPs for the small, medium, and large superstructures, respectively. Also, the observations suggest that the small and medium superstructures have monolayer coverage of gold nanoparticles while the large superstructures are consistent with two layers of NPs. Tabulated gold dielectric constants from Johnson and Christy were used, with a correction to the imaginary part of the dielectric constant to include for surface scattering of the conduction electrons.<sup>13</sup> The refractive index  $n$  of the peptide core was chosen to be 1.6, a typical value used

previously.<sup>14</sup> The surrounding medium was assumed to be water with  $n=1.33$ .

Normalized extinction spectra calculated using the GMM method are shown in Fig. S12†. The simulated extinction spectra for the small superstructures peak at 540 nm, which is quite close to the experimental value, 550 nm. The plasmon maxima for the larger superstructures are red-shifted as expected, however the red shift is significantly smaller than what is observed in the experiments (Fig. 2a). One possible explanation for this difference in the amount of plasmon band red-shifting is that the real size of the interparticle gaps may be smaller than those measured in the TEM images. Indeed, most interparticle gaps are not clearly defined in the TEM images. To modify the electrodynamic modeling we performed calculations using GMM with smaller gaps. As shown in Fig. S12†, even with gaps decreased down to 1 nm, the calculated SPRs, located at 570 nm and 640 nm for medium and large superstructures, are still far from the experimental observations (670 nm and 740 nm).

For gaps of less than 1 nm, classical theories such as the GMM method are no longer valid due to the onset of quantum effects. Nordlander and co-workers studied the plasmon resonance properties of a nanoparticle dimer using time-dependent density functional theory (TD-DFT), and found that the red-shifting trend with decreasing interparticle gap is reversed for dimer separations below 1 nm.<sup>15</sup> There is also experimental evidence supporting this result.<sup>12d, 16</sup> Additional resonances, denoted charge transfer plasmons, also appear for small gaps,<sup>17</sup> including one that is red-shifted relative to the red-most classical resonance. Charge transfer plasmons are often described as arising from electron tunnelling between the nanoparticles, and as a consequence there is extreme sensitivity of the energies of these resonances to gap size. Because of this, it is impractical to estimate spectra based on such models.

A much simpler explanation is that the gold NPs are touching or may be partially fused together instead of being fully isolated from each other (Fig. 1b, d, and f). This leads to the formation of a quasi-continuous gold shell with defects such as pinholes. In a previous study on the optical properties of metal nanoshells, Hao et al. found that the effect of such small pinholes on the extinction maxima is small.<sup>18</sup> Thus, in the extinction spectrum simulation, the defected quasi-continuous gold shell can be simplified to a perfect continuous spherical shell. The thickness of the equivalent gold shell is determined by the average diameter of the component gold NPs which we take to be 8.5 nm and 20 nm for the medium and large superstructures, respectively. The optical response of the resulting core-shell structure can readily be studied by Mie theory.<sup>19</sup>

The extinction spectra calculated using this continuous shell model are shown in Fig. S13†. The medium and large superstructures show plasmon resonances at 675 nm and 730 nm, respectively, which are in quite good agreement with the experimentally observed values (670 nm and 740 nm). Fig. 2b shows calculated spectra analogous to the corresponding experiments in Fig. 2a, with the small superstructure calculated using GMM while the medium and large superstructures are from Mie theory (and we note that the small superstructure is also well-described as a continuous shell with a 7.0 nm thickness). The comparison between theory and experiment is excellent, thus indicating that the continuous shell model is an accurate representation of the plasmonic properties of the superstructures. Differences in the plasmon widths in Fig. 2a and 2b are due to polydispersity, as mentioned earlier.

## Conclusions

In summary, hollow gold nanoparticle superstructures with varied sizes (~40 nm, ~75 nm, ~150 nm) and surface plasmon resonance (SPR) responses have been prepared by using a single peptide conjugate, C<sub>6</sub>-AA-PEP<sub>Au</sub>. The SPR bands red-shift and broaden as the diameters of the spheres and individual gold NPs increase. Medium (75.3 ± 12.4 nm) and large (149.7 ± 30.8 nm) spheres each display broad SPR peaks in the NIR window (650-900 nm), pointing toward their potential for biological applications. A shell model was used to successfully simulate the optical properties of these materials. The success of this model in explaining the large SPR red-shifting of the medium and large spheres implies that they are likely composed of a quasi-continuous shell structure with defects such as pinholes. Moreover, the shell model can be used to develop design rules for synthesizing new superstructures.

## Acknowledgements

C.Z., A.M., C.S. and N.L.R. are grateful for financial support from the National Science Foundation (DMR-0954380, NLR) and the Air Force Office of Scientific Research (FA9550-11-1-0275, NLR). They also thank the Biology Department and the MEMS Department for provision of access to TEM. Y.Z. and G.C.S. are supported by the Department of Energy, Basic Energy Sciences (DE-SC0004752, GSC) and the Air Force Office of Scientific Research (FA9550-11-1-0275, GSC). Computing resources were provided by the Quest high performance computing facility at Northwestern University.

## Notes and references

<sup>a</sup>Department of Chemistry, University of Pittsburgh, Pittsburgh, Pennsylvania 15260, United States. E-mail: nrosi@pitt.edu

<sup>b</sup>Department of Chemistry, Northwestern University, Evanston, Illinois 60208-3113, United States. Email: schatz@chem.northwestern.edu

†Chen Zhang and Yong Zhou contributed equally to this work. Electronic Supplementary Information (ESI) available: Experimental procedures and fig. S1-S15. See DOI: 10.1039/c000000x/

- (a) F. Caruso, R. A. Caruso and H. Mohwald, *Science*, 1998, **282**, 1111; (b) C. Song, G. Zhao, P. Zhang and N. L. Rosi, *J. Am. Chem. Soc.*, 2010, **132**, 14033; (c) L. Hwang, G. Zhao, P. Zhang and N. L. Rosi, *Small*, 2011, **7**, 1939; (d) C. Song, Y. Wang and N. L. Rosi, *Angew. Chem. Int. Ed.*, 2013, **52**, 3993; (e) R. J. Hickey, A. S. Haynes, J. M. Kikkawa and S.-J. Park, *J. Am. Chem. Soc.*, 2011, **133**, 1517; (f) J. Song, L. Cheng, A. Liu, J. Yin, M. Kuang and H. Duan, *J. Am. Chem. Soc.*, 2011, **133**, 10760; (g) J. Song, J. Zhou and H. Duan, *J. Am. Chem. Soc.*, 2012, **134**, 13458; (h) J. Song, L. Pu, J. Zhou, B. Duan and H. Duan, *ACS Nano*, 2013, **7**, 9947; (i) J. He, Y. Liu, T. Babu, Z. Wei and Z. Nie, *J. Am. Chem. Soc.*, 2012, **134**, 11342; (j) J. He, X. Huang, Y.-C. Li, Y. Liu, T. Babu, M. A. Aronova, S. Wang, Z. Lu, X. Chen and Z. Nie, *J. Am. Chem. Soc.*, 2013, **135**, 7974; (k) Y. C. Yeh, R. Tang, R. Mout, Y. Jeong and V. M. Rotello, *Angew. Chem. Int. Ed.*, 2014, **53**, 5137; (l) P. Huang, J. Lin, W. Li, P. Rong, Z. Wang, S. Wang, X. Wang, X. Sun, M. Aronova, G. Niu, R. D. Leapman, Z. Nie and X. Chen, *Angew. Chem. Int. Ed.*, 2013, **52**, 13958; (m) K. Niikura, N. Iyo, T. Higuchi, T. Nishio, H. Jinnai, N. Fujitani and K. Ijiri, *J. Am. Chem. Soc.*, 2012,

- 134, 7632; (n) C. Sanson, O. Diou, J. Thévenot, E. Ibarboure, A. Soum, A. Brûlet, S. Miraux, E. Thiaudière, S. Tan, A. Brisson, V. Dupuis, O. Sandre and S. Lecommandoux, *ACS Nano*, 2011, **5**, 1122.
- 2 (a) S. Mühlig, A. Cunningham, S. Scheeler, C. Pacholski, T. Bürgi, C. Rockstuhl and F. Lederer, *ACS Nano*, 2011, **5**, 6586; (b) S. N. Sheikholeslami, H. Alaeian, A. L. Koh and J. A. Dionne, *Nano Lett.*, 2013, **13**, 4137.
- 3 R. Weissleder, *Nature Biotech.*, 2001, **19**, 316.
- 4 (a) N. A. Kotov and F. Stellacci, *Adv. Mater.*, 2008, **20**, 4221; (b) Z. H. Nie, A. Petukhova and E. Kumacheva, *Nature Nanotech.*, 2010, **5**, 15; (c) M. R. Jones, K. D. Osberg, R. J. Macfarlane, M. R. Langille, and C. A. Mirkin, *Chem. Rev.*, 2011, **111**, 3736.
- 5 C.-L. Chen, P. Zhang, N. L. Rosi, *J. Am. Chem. Soc.*, 2008, **130**, 13555.
- 6 (a) S. R. Whaley, D. S. English, E. L. Hu, P. F. Barbara and A. M. Belcher, *Nature*, 2000, **405**, 665; (b) J. M. Slocik, M. O. Stone and R. R. Naik, *Small*, 2005, **1**, 1048; (c) D. B. Pacardo, M. Sethi, S. E. Jones, R. R. Naik and M. R. Knecht, *ACS Nano*, 2009, **3**, 1288; (d) C. Y. Chiu, Y. J. Li, L. Y. Ruan, X. C. Ye, C. B. Murray and Y. Huang, *Nature Chem.*, 2011, **3**, 393; (e) M. B. Dickerson, K. H. Sandhage and R. R. Naik, *Chem. Rev.*, 2008, **108**, 4935; (f) C. L. Chen and N. L. Rosi, *Angew. Chem. Int. Ed.*, 2010, **49**, 1924.
- 7 (a) C. L. Chen and N. L. Rosi, *J. Am. Chem. Soc.*, 2010, **132**, 6902; (b) L. Hwang, C.-L. Chen and N. L. Rosi, *Chem. Commun.*, 2011, **47**, 185; (c) C. Y. Song, M. G. Blaber, G. P. Zhao, P. J. Zhang, H. C. Fry, G. C. Schatz and N. L. Rosi, *Nano Lett.*, 2013, **13**, 3256; (d) C. Zhang, C. Song, H. C. Fry and N. L. Rosi, *Chem. Eur. J.*, 2014, **20**, 941.
- 8 (a) A. Habib, M. Tabata and Y. G. Wu, *Bull. Chem. Soc. Jpn.*, 2005, **78**, 262; (b) J. P. Xie, J. Y. Lee, and D. I. C. Wang, *Chem. Mater.*, 2007, **19**, 2823.
- 9 H. Wang, J. Kundu and N. J. Halas, *Angew. Chem. Int. Ed.*, 2007, **46**, 9040.
- 10 (a) E. Ozbay, *Science*, 2006, **311**, 189; (b) Z. Tang, Y. Wang, P. Podsiadlo and N. A. Kotov, *Adv. Mater.*, 2006, **18**, 3203.
- 11 S. J. Oldenburg, R. D. Averitt, S. L. Westcott and N. J. Halas, *Chem. Phys. Lett.*, 1998, **288**, 243.
- 12 (a) Y. L. Xu, *Appl. Optics*, 1995, **34**, 4573; (b) Y. L. Xu, *Appl. Optics*, 1997, **36**, 9496; (c) Y. L. Xu and R. T. Wang, *Phys. Rev. E*, 1998, **58**, 3931; (d) J. H. Yoon, Y. Zhou, M. G. Blaber, G. C. Schatz and S. Yoon, *J. Phys. Chem., Lett.*, 2013, **4**, 1371.
- 13 (a) P. B. Johnson and R. W. Christy, *Phys. Rev. B*, 1972, **6**, 4370; (b) U. Kreibig and Vonfrags, *Z. Phys.*, 1969, **224**, 307; (c) E. A. Coronado and G. C. Schatz, *J. Chem. Phys.*, 2003, **119**, 3926; (d) A. Moroz, *J. Phys. Chem. C*, 2008, **112**, 10641.
- 14 B. M. Reinhard, M. Siu, H. Agarwal, A. P. Alivisatos and J. Liphardt, *Nano Lett.*, 2005, **5**, 2246.
- 15 J. Zuloaga, E. Prodan and P. Nordlander, *Nano Lett.*, 2009, **9**, 887.
- 16 S. F. Tan, L. Wu, J. K. W. Yang, P. Bai, M. Bosman and C. A. Nijhuis, *Science*, 2014, **343**, 1496.
- 17 R. Esteban, A. G. Borisov, P. Nordlander and J. Aizpurua, *Nature Commun.*, 2012, **3**.
- 18 E. Hao, S. Y. Li, R. C. Bailey, S. L. Zou, G. C. Schatz and J. T. Hupp, *J. Phys. Chem. B*, 2004, **108**, 1224.
- 19 C. F. Bohren and D. R. Huffman, *Absorption and scattering of light by small particles*, Wiley Interscience, New York, 1983.